Magnetic flux generation and wave emissions during coalescence of magnetic islands in pair plasmas

J. I. Sakai, T. Haruki, and Y. Kazimura
Laboratory for Plasma Astrophysics, Faculty of Engineering, Toyama University, 3190, Gofuku, Toyama 930-8555, Japan
(Received 20 November 1998; revised manuscript received 16 February 1999)

It is shown by using a two-dimensional fully relativistic electromagnetic particle-in-cell code that the tearing instability in a current sheet of pair plasmas is caused by Landau resonances of both electrons and positrons. Strong magnetic flux can be generated during coalescence of magnetic islands in the nonlinear phase of the tearing instability. The magnetic flux produced in an O-type magnetic island is caused by the counterstreaming instability found by Kazimura *et al.* [Astrophys. J. Lett. **498**, L183 (1998); J. Phys. Soc. Jpn. **67**, 1079 (1998)]. It is also shown that charge separation with a quadrupolelike structure is generated from the localized strong magnetic flux. During the decay of the quadrupolelike charge structure as well as the magnetic flux, there appear wave emissions with high-frequency electromagnetic waves and Alfvén waves as well as Langmuir waves. [S1063-651X(99)06607-6]

PACS number(s): 52.35.−g

I. INTRODUCTION

Magnetic reconnection [1] in plasmas is one of important energy conversion processes in plasmas from magnetic field energy to plasma kinetic energy as well as high-energy particles. Magnetic islands formed through the tearing instability in an unstable current sheet are unstable against the coalescence instability [2]. The coalescence instability is an ideal magnetohydrodynamic (MHD) instability in which parallel currents attract each other and to coalesce into larger units through magnetic reconnection. A lot of works on the coalescence dynamics in electron-ion plasmas have been published both in the MHD model [3] and the collisionless model [4]. Pritchett [5] reported a new effect on the magnetic flux generation during coalescence of magnetic islands in electron-ion plasma, and showed that during the nonlinear stage of the merging process of two magnetic islands, a quadrupole out-of-plane magnetic field structure with a size of the ion skin depth is formed. On the other hand, study on magnetic reconnection [6] and coalescence dynamics [7] in electron-positron (pair) plasmas has begun under some motivations in astrophysical plasmas.

In the present paper we report simulation results on the tearing instability as well as on the coalescence dynamics of magnetic islands formed in a current sheet of pair plasmas, using a two-dimensional (2D) fully relativistic particle-in-cell (PIC) code. We found that the tearing instability in a current sheet in pair plasmas is caused by Landau resonances of both electrons and positrons. In the nonlinear phase of the tearing instability, strong localized magnetic flux with a size of the order of the electron skin depth (c/ω_{pe}) can be generated by the counterstreaming instability during coalescence of magnetic islands, whose process was recently investigated by both theory and simulation [8]. It is also found that charge separation caused by the localized magnetic flux has a quadrupolelike structure. During the decay phase of the magnetic flux and charge separation, there appear wave emissions of electromagnetic and Langmuir waves from the localized magnetic flux region. The strongly excited wave among them is the Alfvén wave propagating along a magnetic field.

The paper is organized as follows: in Sec. II we present our simulation model. In Sec. III we present the simulation results. In Sec. IV we summarize our results.

II. SIMULATION MODEL

The simulation code used here is a $2\frac{1}{2}$-dimensional code, assuming that the physical quantities are constant in $z(\partial/\partial z = 0)$, which was modified from the three-dimensional, fully electromagnetic, and relativistic TRISTAN code [9]. The system size is $L_x = 140\Delta$ and $L_y = 200\Delta$, where Δ $(=1)$ is the grid size. Periodic boundary conditions are imposed on particles and fields. There are 2.8×10^6 electron-positron pairs filling the entire domain uniformly and that keeps the domain charge neutral. Hence, the average particle number density is about 100 per cell. Due to limitations of the periodic boundary conditions, double current sheets are set up of the antiparallel magnetic field configuration, namely,

$$B_x(y) = B_0\left[\tanh\left(\frac{y-60}{L}\right) - \tanh\left(\frac{y-140}{L}\right)\right], \qquad (1)$$

$$j_z(y) = \frac{cB_0}{4\pi L}\left[\mathrm{sech}^2\left(\frac{y-60}{L}\right) - \mathrm{sech}^2\left(\frac{y-140}{L}\right)\right], \qquad (2)$$

where $L(=20\Delta)$ is the width of the current sheets. The center lines of the current sheets are located at $y=60$ and $y=140$ in the x-y plane, respectively. The initial state is characterized by complete neutrality ($\mathbf{E}_0 = 0$) everywhere in the domain. Other parameters are as follows: the mass ratio between an electron and a positron, $m_e/m_p = 1$; the simulation time step $\omega_{pe}\Delta t = 0.052$; the plasma frequency $\omega_{pe} = \sqrt{e^2 n/\epsilon_0 m_e}$ $(\epsilon_0 = 1)$ to the electron cyclotron frequency $\omega_e = eB_0/m_e$, $\omega_{ce}/\omega_{pe} = 1.89$ for maximum magnetic field strength B_0, the ratio of the electron thermal velocity parallel to the magnetic field B_x to the light velocity $v_{te}/c = \sqrt{2\kappa T_e/m_e}/c = 0.094$; the Debye length $\lambda_{De} = 0.89\Delta$; the

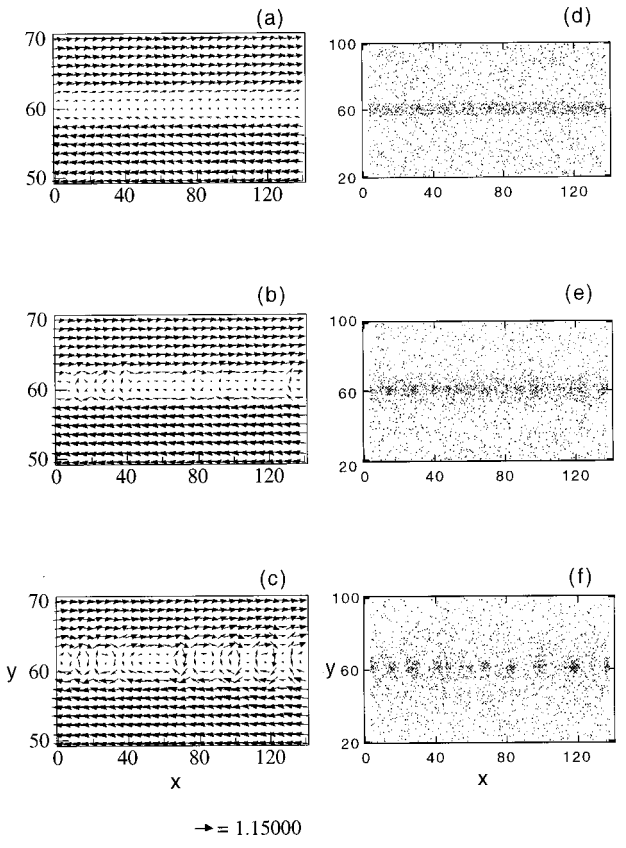

FIG. 1. Vector plots of the magnetic fields B_x and B_y in the x-y plane: (a) $\omega_{pe}t=4.2$, (b) $\omega_{pe}t=6.3$, and (c) $\omega_{pe}t=8.4$. The time development of the electron spatial distributions in the x-y plane, in which a fraction of 1/500 of all electrons is plotted: (d) $\omega_{pe}t=4.2$, (e) $\omega_{pe}t=6.3$. and (f) $\omega_{pe}t=8.4$.

skin depth $c/\omega_{pe}=9.6\Delta$; the plasma beta value $\beta=0.002$; the temperature of electrons T_e to the temperature of positrons T_p, $T_e/T_p=1$. The gyroradius for both thermal electrons and positrons is $\rho_e=\rho_p=0.47\Delta$ for maximum magnetic field strength B_0.

III. SIMULATION RESULTS

A. Tearing instability in pair plasmas

As is well known, double current sheets are unstable against the tearing instability, which can produce small scale magnetic islands with the order of the width of the current sheet. Here we show the simulation results obtained in the current sheet, whose center is located at $y=60$. Figures 1(a)–1(c) show the vector plots of the magnetic fields B_x and B_y in the x-y plane at $\omega_{pe}t=4.2$ (a), $\omega_{pe}t=6.3$ (b), and $\omega_{pe}t=8.4$ (c), respectively. Figures 1(d)–1(f) show time development of the electron spatial distributions in the x-y plane at $\omega_{pe}t=4.2$ (d), $\omega_{pe}t=6.3$ (e), and $\omega_{pe}t=8.4$ (f), respectively. As seen in Figs. 1(d)–1(f), the current becomes unstable against the tearing instability, leading to the formation of the electron bunching associated with magnetic islands. We find the linear growth rate of the tearing instability from the time history of the magnetic field energy B_y^2 shown in Fig. 2. The observed growth rate is about $\gamma/\omega_{pe}=0.67$, whose value is obtained from the time interval of $3.0 \leqslant \omega_{pe}t \leqslant 5.0$ in Fig. 2. Figures 3 show the three components of the electron velocity distributions at $\omega_{pe}t=4.2$.

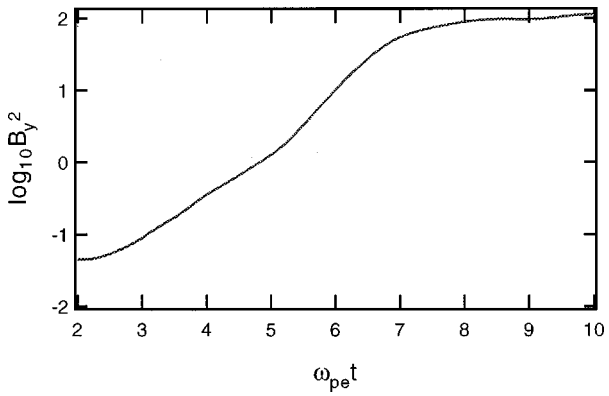

FIG. 2. Time development of magnetic field energy B_y^2. The growth rate of the tearing instability is calculated in the time interval of $3.0 \leqslant \omega_{pe}t \leqslant 5.0$.

We compare the simulation result with the theoretical growth rate of the tearing mode instability due to Landau resonances [10]. In the present simulation of pair plasmas,

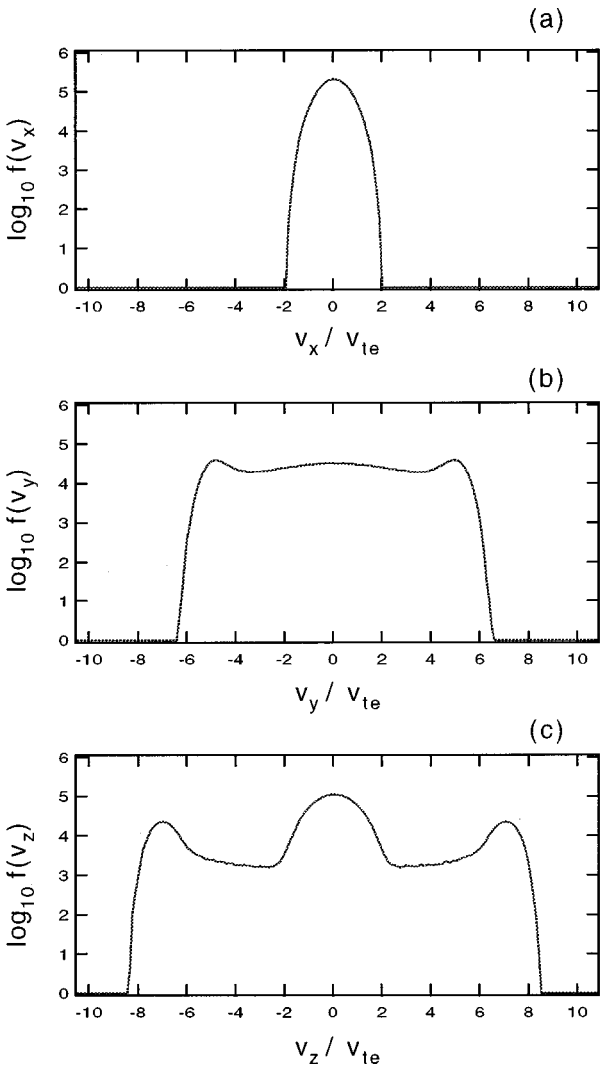

FIG. 3. Three components of the electron velocity distribution at $\omega_{pe}t=4.2$.

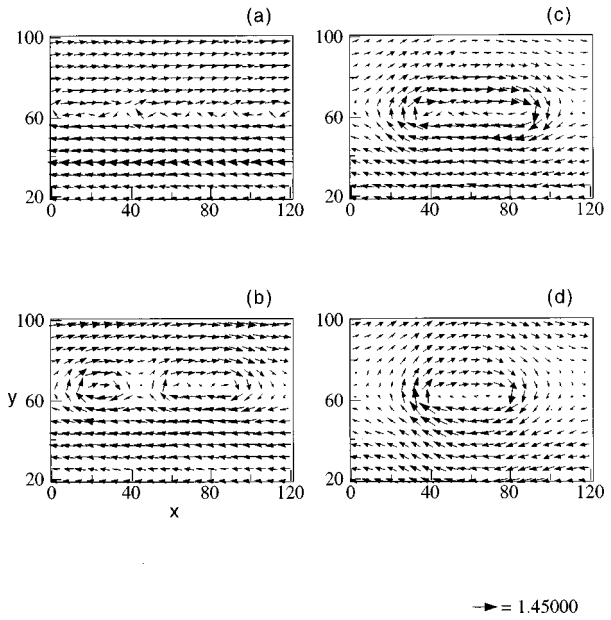

FIG. 4. Time development of magnetic islands produced in a current sheet: (a) $\omega_{pe}t=10.54$, (b) $\omega_{pe}t=21.08$, (c) $\omega_{pe}t=26.35$, and (d) $\omega_{pe}t=31.62$.

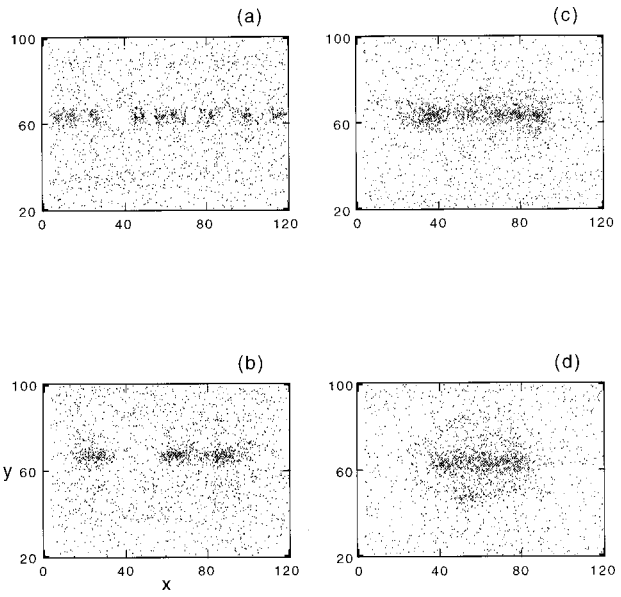

FIG. 5. Time development of the electron spatial distribution near a current sheet, in which a fraction of 1/500 of all electrons is plotted: (a) $\omega_{pe}t=10.54$, (b) $\omega_{pe}t=21.08$, (c) $\omega_{pe}t=26.35$, and (d) $\omega_{pe}t=31.62$.

both electrons and positrons can contribute to Landau resonances in the current sheet, therefore the linear growth rate of the tearing instability in pair plasmas becomes just twice of the electron tearing instability in the electron-ion plasmas. The growth is given by $\gamma/\omega_{pe}=4\pi^{1/2}(v_{te}/\alpha c)(v_{te}\omega_{pe}/\omega_{ce}\alpha c)^{3/2}(1-k^2L^2)$, where we used the thickness L of the current sheet as $L=\alpha c/\omega_{pe}$. From the present simulation data, we obtain $\alpha=0.5$, $v_{te}/c=0.3$, and $\omega_{pe}/\omega_{ce}=0.5$. Therefore we find the theoretical growth rate of the tearing instability in pair plasmas as $(\gamma/\omega_{pe})_{\text{theory}}=0.7$, which agrees well with the above simulation result. We may conclude that the tearing instability in pair plasmas is due to a fully kinetic effect of Landau resonances of both electrons and positrons, in contrast with other effects such as resistivity [6] and electron inertia [11].

B. Generation of magnetic flux during coalescence of magnetic islands

Figure 4(a) shows the formation of several magnetic islands at $\omega_{pe}t=10.54$. At $\omega_{pe}t=21.08$ [see Fig. 4(b)] two magnetic islands are formed, and finally a single large magnetic island is produced, as seen in Figs. 4(c) at $\omega_{pe}t=26.35$ and Fig. 4(d) at $\omega_{pe}t=31.62$. Figure 5 shows the time development of the electron spatial distribution in the x-y plane, whose time sequence corresponds to the previous vector plots of the magnetic field. In these figures only a fraction of 1/500 of all electrons is plotted. As seen in these figures, the magnetic islands correspond to high density plasma blobs. During the coalescence of two magnetic islands from $\omega_{pe}t=21.08$ [see Fig. 4(b)] to $\omega_{pe}t=26.35$ [see Fig. 4(c)], the left plasma blob is attracted to the right large blob and eventually merges into one blob. The colliding velocity of the left plasma blob is about $0.2c$.

We now investigate the process of the collision of two plasma blobs in more detail. Figure 6 shows three snapshots at $\omega_{pe}t=28.46$, 31.62, and 36.89, in which the left column [Figs. 6(a-1)–6(a-3)] shows the development of magnetic flux B_z. In the middle column [Figs. 6(b-1)–6(b-3)] the vector plots of magnetic fields are shown, and in the right column [Figs. 6(c-1)–6(c-3)] the spatial distributions of the electric charge density $(\rho_+-\rho_-)$ in the x-y plane are presented. As seen in Fig. 6(a-1), there is no magnetic flux in the early phase of coalescence of magnetic islands. However, as seen in Fig. 6(a-2) there appears strong magnetic flux generation with a pair polarity just near the center of the merged magnetic island. In the late phase at $\omega_{pe}t=36.89$ the generated magnetic flux can diffuse in space and decay. The origin of the strong magnetic flux generation is due to the countersteaming instability, which was recently investigated by Kazimura *et al.* [8]. It is found that the countersteaming instability with the narrow transverse size of the order of the electron skin depth can cause strong magnetic flux associated with the charge separation. As seen in Fig. 6(c-2), the charge separation with a quadrupolelike structure occurs in coincidence with the formation of the magnetic flux. This is due to the Larmor motions of colliding plasma streams under the strong localized negative magnetic flux B_z. In this simulation the typical Larmor radius is about $0.6\ c/\omega_{pe}$ by using the colliding velocity $0.2c$ and the generated magnetic field strength $B_z=0.4$ at $\omega_{pe}t=30$. This value agrees well with the observed size of the charge separation. Associated with the decay of the generated magnetic flux, the charge separation also becomes too weak to keep the charge neutrality in the x-y plane, as seen in Fig. 6(c-3).

C. Generation of waves

In the preceding subsection we showed the generation of the strong localized magnetic flux, which can cause the charge separation with the quadrupolelike structure. In the decay phase of the generated magnetic flux as well as the charge separation it is expected that there occurs a strong generation of waves. In order to study the wave emission

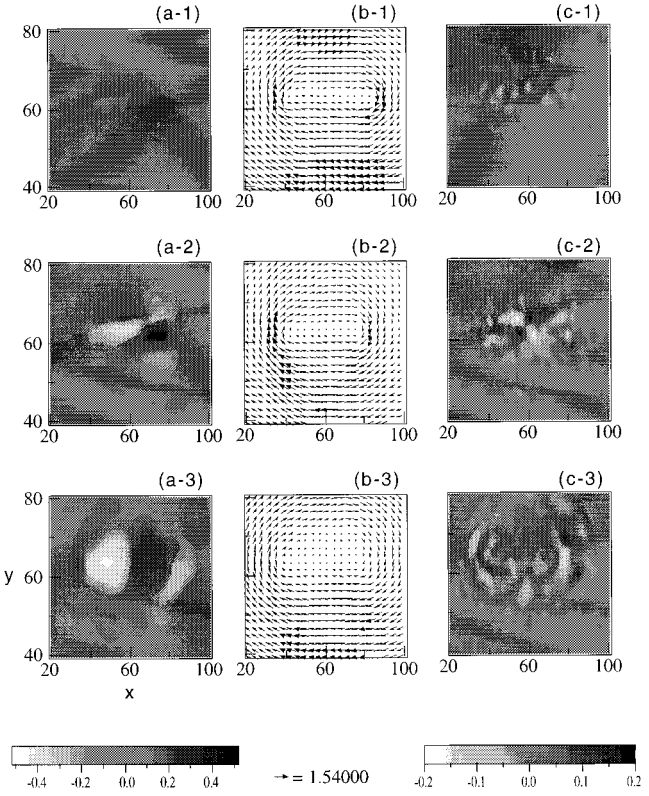

FIG. 6. Generation and decay of magnetic flux B_z in an O-type magnetic island: (a-1) $\omega_{pe}t=28.46$, (a-2) $\omega_{pe}t=31.62$, and (a-3) $\omega_{pe}t=36.89$. The time development of a coalesced magnetic island: (b-1) $\omega_{pe}t=28.46$, (b-2) $\omega_{pe}t=31.62$, and (b-3) $\omega_{pe}t=36.89$. The generation and decay of the charge separation during coalescence of magnetic islands: (c-1) $\omega_{pe}t=28.46$, (c-2) $\omega_{pe}t=31.62$, and (c-3) $\omega_{pe}t=36.89$.

process and to get the dispersion relations of the excited waves, we performed a 2D Fourier analysis in the x direction and the time interval $0\leqslant\omega_{pe}t\leqslant 54$ with 1024 time data points for the electric field E_y on $y=45\Delta$ and the magnetic field B_z on $y=75\Delta$.

Figure 7(a) shows the dispersion relation along the magnetic field B_x. We find that there occur high-frequency electromagnetic waves, which can be produced from the decaying charge separation in the O-type magnetic island. Figure 7(c) shows the time history of the electric field energy E_y^2 which can be obtained from the data of Fig. 7(a), by performing the inverse Fourier transformation. As seen in this figure, the high-frequency electromagnetic waves can be produced just after formation of the strong charge separation in the magnetic island. In the decay phase of the structure of the charge density, the emission of the electromagnetic waves is enhanced in time.

Figure 7(b) shows the dispersion relation of the magnetic field B_z along the magnetic field B_x. The strongest emission occurs near at $\omega/\omega_{pe}=0.23$ and $kc/\omega_{pe}=0.93$. This branch of the waves corresponds to Alfvén waves propagating along the magnetic field. In Fig. 7(b) three theoretical dispersion curves of the Alfvén waves, which are obtained from the dispersion relation, $(kc/\omega)^2=1-2\omega_{pe}^2/(\omega^2-\omega_{ce}^2)$ with (1) $\omega_{ce}/\omega_{pe}=0.5$, (2) $\omega_{ce}/\omega_{pe}=0.4$, and (3) $\omega_{ce}/\omega_{pe}=0.3$, are plotted by the solid lines. The strongest emission obtained from the simulation is located between the theoretical dispersion curve (1) and (2), as seen from Fig. 7(b). We conclude from the simulation data that the ratio $\omega_{ce}/\omega_{pe}=0.45$ is a reasonable value to fit with the theoretical dispersion curve. Figure 7(d) shows the time history of the magnetic field energy B_z^2. which can be obtained from the data of Fig. 7(b), by performing the inverse Fourier transformation. As seen in this figure, the Alfvén waves can be excited in association with the decay of the strongly generated localized magnetic flux in the center of the magnetic island. The amplitude $\delta B/B_0$ of the excited Alfvén waves is about 0.1 and quite strong.

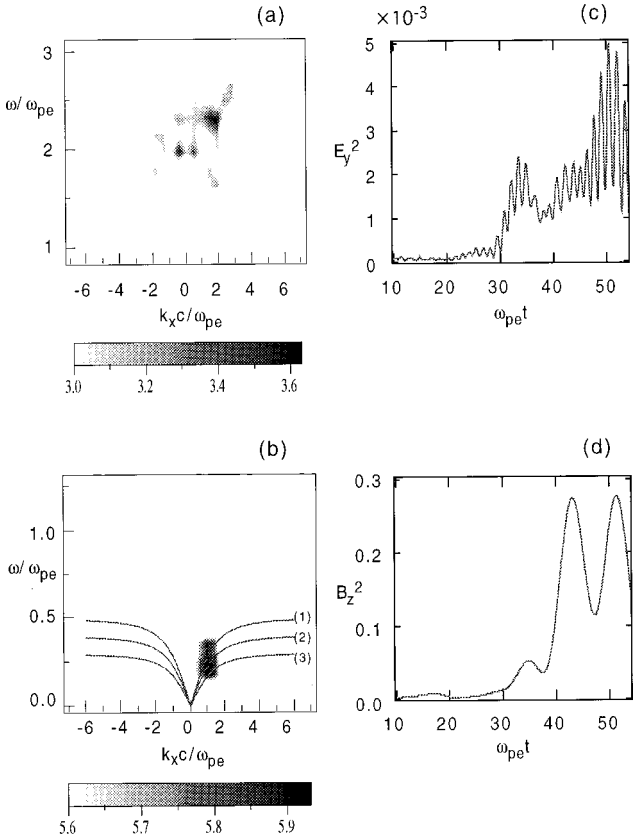

FIG. 7. Dispersion relation (a) of electromagnetic waves associated with the electric field E_y, and the dispersion relation (b) of Alfvén waves associated with the magnetic field B_z propagating along a magnetic field B_x. In (b) three solid curves show the theoretical dispersion relations of the Alfvén waves for (1) $\omega_{ce}/\omega_{pe}=0.5$, (2) $\omega_{ce}/\omega_{pe}=0.4$, and (3) $\omega_{ce}/\omega_{pe}=0.3$. (c) The time history of the electric field energy E_y^2 associated with the electromagnetic waves obtained from (a). (d) The time history of the magnetic field energy B_z^2 associated with the Alfvén waves obtained from (b).

IV. SUMMARY

We have shown by using a 2D fully relativistic electromagnetic particle-in-cell (PIC) code that the tearing instability in a current sheet of pair plasmas is caused by Landau resonances of both electrons and positrons. Strong magnetic flux can be generated during coalescence of magnetic islands in the nonlinear phase of the tearing instability. The magnetic flux generated in an O-type magnetic island is caused by the counterstreaming instability found by Kazimura *et al.* [8]. We also presented that the charge separation with a quadrupolelike structure is produced due to Larmor motions of

counterstreaming particles under the localized strong magnetic flux. During the decay of the quadrupolelike charge structure as well as the magnetic flux, there appear strong wave emissions with high-frequency electromagnetic waves and Alfvén waves as well as Langmuir waves. In this paper we presented simulation results of a case that the width of a current sheet is the order of the electron skin depth. When the width of the current sheet becomes wider than the electron skin depth, the transverse scale of the magnetic islands also becomes large. In this situation the structure of the magnetic flux generated during coalescence of magnetic islands becomes more complicated than the case shown in this paper. The details of this study is under preparation. These physical processes associated with generation of magnetic flux and wave emissions could occur in a current sheet of electron-ion plasmas.

ACKNOWLEDGMENT

J. I. Sakai thanks the Densoku company for their support.

[1] J. W. Dungey, Phys. Rev. Lett. **6**, 47 (1961); P. A. Sweet, Proc. IAU Symp. **6**, 123 (1958); E. N. Parker, J. Geophys. Res. **79**, 1558 (1957); H. E. Petschek, AAS-NASA Symposium on Physics of Solar Flares [NASA Spec. Publ. **50**, 425 (1964)]; V. M. Vasyliunas, Rev. Geophys. Space Phys. **13**, 303 (1975); D. Biskamp, *Nonlinear Magnet Hydrodynamics* (Cambridge University Press, Cambridge, England, 1993), Chap. 6; J. I. Sakai and C. de Jager, Space Sci. Rev. **77**, 1 (1996).

[2] J. M. Finn and P. K. Kaw, Phys. Fluids **20**, 72 (1977).

[3] P. L. Pritchett and C. C. Wu, Phys. Fluids **22**, 2140 (1979).

[4] P. L. Pritchett, Phys. Fluids B **4**, 3371 (1992).

[5] P. L. Pritchett, Phys. Plasmas **2** (7), 2664 (1995).

[6] P. K. Shukla, M. Y. Yu, and V. N. Pavlenko, Astrophys. Space Sci. **134**, 181 (1987); E. G. Blackman and G. B. Field, Phys. Rev. Lett. **71**, 3481 (1993); **72**, 494 (1994).

[7] J. Zhao, J. I. Sakai, and K. I. Nishikawa, Phys. Plasmas **3** (3), 844 (1996).

[8] Y. Kazimura, J. I. Sakai, T. Neubert, and S. V. Bulanov, Astrophys. **498**, L183 (1998); J. Phys. Soc. Jpn. **67**, 1079 (1998).

[9] O. Buneman, in *Computer Space Plasma Physics, Simulation Techniques and Softwares*, edited by H. Mastumoto and Y. Omura (Terra Scientific, Tokyo, 1993), p. 67.

[10] G. Laval, R. Pellat, and M. Vullemin, Plasma Phys. Controlled Nucl. Fusion Res. **2**, 259 (1966); A. A. Galeev, *Basic Plasma Physics*, edited by M. N. Rosenbluth and R. Z. Sagdeev (North-Holland, Amsterdam, 1984), Vol. 2, Chap. 6.2, p. 314.

[11] D. Biskamp, E. Schwarz, and J. F. Drake, Phys. Plasmas **4**, 1002 (1997).